

41044
11

OBJECTIVE DETERMINATION OF IMAGE END-MEMBERS IN SPECTRAL MIXTURE ANALYSIS OF AVIRIS DATA

Stefanie Tompkins, John F. Mustard, Carle M. Pieters, Donald W. Forsyth
Dept. Geol. Sci., Box 1846, Brown University, Providence, RI 02912

INTRODUCTION

Spectral mixture analysis has been shown to be a powerful, multifaceted tool for analysis of multi- and hyper-spectral data (Adams et al., 1986; Smith et al., 1990). Applications to AVIRIS data have ranged from mapping soils and bedrock to ecosystem studies (e.g. Gamon et al., 1993; Roberts et al., 1993; Mustard et al., 1993; Kruse et al., 1993). During the first phase of the approach, a set of end-members are selected from an image cube (image end-members) that best account for its spectral variance within a constrained, linear least squares mixing model. These image end-members are usually selected using *a priori* knowledge and successive trial and error solutions to refine the total number and physical location of the end-members. However, in many situations a more objective method of determining these essential components is desired. We approach the problem of image end-member determination objectively by using the inherent variance of the data. Unlike purely statistical methods such as factor analysis, this approach derives solutions that conform to a physically realistic model.

DAMPED LEAST SQUARES MODEL

The underlying assumption of spectral mixture analysis is that each pixel on the surface is a physical mixture of several components, and the spectrum of the mixture is a linear combination of the end-member reflectance spectra. The spectral variability of a scene is thus modeled as a linear combination of a small number of image end-members. The fundamental equations of spectral mixture analysis are:

$$\sum_b R_b = \sum_b \sum_i r_{ib} f_i + \sum_b E_b \quad (1) \quad \text{and} \quad \sum_i f_i = 1.0 \quad (2)$$

where f_i is the fractional abundance of end-member i in the pixel, R_b is the total reflectance of the pixel in band b , r_{ib} is the reflectance of end-member i in band b , and E_b is the residual error in band b . In a typical spectral mixing analysis, the end-members are prescribed and the fractional abundances and errors are then calculated for each pixel, through a simple least squares inversion of the form:

$$\underline{m} = (\underline{G}^T \underline{G})^{-1} \underline{G}^T \underline{d} \quad (3)$$

The matrix \underline{G} consists of the partial derivatives of the model equations given by (1) and (2). The vectors \underline{d} and \underline{m} represent the data (R_b) and the model parameters (f_i) respectively. A two-dimensional graphical representation of mixture analysis is shown in Figure 1. The image end-members (indicated by squares) should reside as close as possible to the boundaries of the data cloud. Fractions that are >1.0 or <0.0 occur for data points that lie outside the region defined by the end-members, and cannot be entirely eliminated no matter how well chosen the image end-members.

Consider, instead, an approach where the end-member spectra are not prescribed, but are treated as unknowns along with the fractional abundances. The model equations are the same as stated above, but because F_i and r_{ib} are both unknowns, they must be

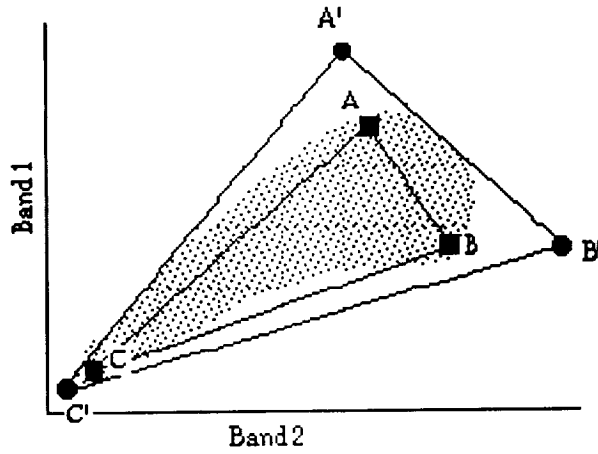


Figure 1: A, B, and C indicate image end-members. A', B', and C' are the model-derived end-members.

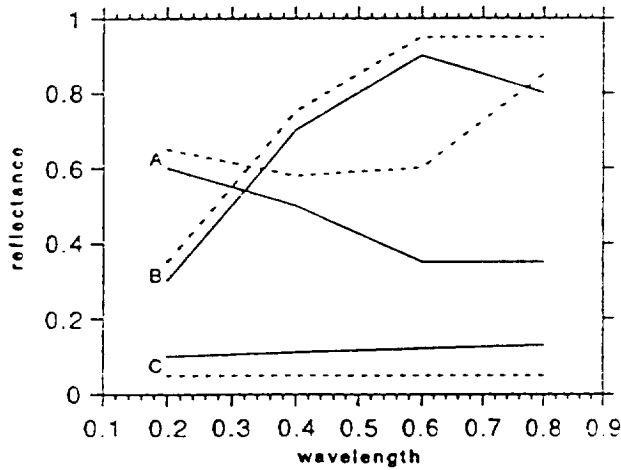


Figure 2: Solid lines represent image end-member spectra. Dashed lines are model-derived virtual end-members.

solved non-linearly. The approach we have chosen employs a damped least squares non-linear inversion technique as presented by Tarantola and Valette (1982). In short, a starting model is provided (a suite of possible end-member spectra, estimated fractional abundances, and the image data to be modeled). Constraints on the solutions are imposed as additional equations (i.e. fractions must sum to 1.0) or as allowable deviations from the starting model (damping of solutions). Both the starting model and the constraints are based on *a priori* knowledge. Each successive iteration of the equations results in a calculated change to the previous model that will reduce the error of the fit. These changes are incorporated and the inversion is run successively until a prescribed error threshold is surpassed, as given by:

$$\underline{m}_{j+1} = \underline{m}_j + \left[\underline{G}_j^T \underline{C}_{nn}^{-1} \underline{G}_j + \underline{C}_{mm}^{-1} \right]^{-1} \left[\underline{G}_j^T \underline{C}_{nn}^{-1} (\underline{d} - \underline{g}(\underline{m}_j)) - \underline{C}_{mm}^{-1} (\underline{m}_j - \underline{m}_0) \right] \quad (4)$$

In this case, the model parameters and G-matrix change with each iteration (\underline{m}_j is the model parameter vector at the j th iteration) and include both f_i and r_{ib} from equations (1) and (2). \underline{C}_{nn} and \underline{C}_{mm} are covariance matrices for the data and the model parameters, respectively. The term $\underline{g}(\underline{m}_j)$ is the predicted value of the data vector when the forward

model is run, so $(\mathbf{d} - \mathbf{g}(\mathbf{m}_j))$ simply describe the residual error. The starting model parameters, found in \mathbf{m}_0 , are included at each iteration to penalize large deviations from the starting model and thus damp the final solution.

The model results are therefore intimately guided by the inherent spectral variability of the data, the starting model, and the constraints imposed on the solutions. The calculated end-member spectra are driven to better bound the data cloud. This is shown in Figure 1 (new end-members indicated by circles). The effects in a spectral sense are illustrated conceptually in Figure 2 (initial end-member spectra are shown by solid lines and calculated end-members by dashed lines). Although the new end-member spectra are not necessarily identical to any pixel spectrum (they can lie outside the data cloud), they provide the best mathematical fit to the whole data set and are determined using a model which is based on a physically realistic description of the surface. One might think of these as *virtual end-members*.

PRELIMINARY RESULTS

Artificial Data Set

This model was developed and refined on a test data set where the end-members and their abundances are known perfectly. This data set provides a working template for establishing the necessary conditions under which the best solution can be derived. The model successfully reproduces the true end-member spectra in the test data sets for a variety of initial conditions, provided that the model is minimally constrained. An additional step in spectral mixture analysis is determining the optimum number of end-members. Using the test data set, model solutions for fewer than and greater than the correct number of spectral end-members were analyzed. When too few end-members were used, the solution failed to meet the original constraints on the model. The residual error steadily declined as the number of end-members increased until the optimum number was reached; thereafter, the improvement in error was statistically insignificant. Thus, the evolution of error and successful satisfaction of model constraints as a function of the number of end-members can be used to threshold the optimum solution. We continue to use the artificial data sets to develop a better understanding of the model, and establish limits on the amount of *a priori* information that is needed to calculate the true end-member spectra.

Lunar CCD Images

The model has also been applied to 8-band CCD images of the lunar crater Bullialdus (Tompkins et al., 1992). This required some restructuring of the program due to the increased number of spectral channels and pixels; however, the model is the same. The starting model is guided by previous investigations (Tompkins et al., 1992; Pieters, 1991). Initial results on small data sets within the image show generally the same results as were obtained with the traditional mixing approach, but provide a much lower rms error and only very rare occurrences of superpositive (>100%) or negative abundances. In mixing models, the best image end-members can be considered those that best describe the data cloud (Figure 1), for all bands simultaneously. As was found with the test data, the nonlinear inversion defines virtual end-members that are outside the data cloud, while still providing a physically reasonable solution.

AVIRIS Data

The model is now applied to an AVIRIS image from the western foothills of the Sierra Nevada. Materials found within the data include dry, grass-covered hills, irrigated

orchards, and a complex substrate with rapidly changing bedrock composition (Mustard, 1993). Because the memory requirements for the model increase multiplicatively with the number of pixels and spectral channels in a data set, the initial application will be to a subset of the image, using a limited number of channels. The fraction images that result from using virtual end-members will be compared to those derived through the traditional mixing model.

One of the strengths of spectral mixture analysis is the ability to calibrate raw data to reflectance by linking the image end-members to reference end-members from a spectral library. This can be especially advantageous when using data from systems with poorly defined characteristics or areas lacking well characterized reference end-members. Though this can lead to non-unique solutions for the reference end-members, common sense and geologic context help govern the choice of library end-members to which the image end-members are calibrated. The data inversion approach presented here may confer a distinct advantage for proceeding to the calibration stage. The virtual end-members are thought to be more spectrally pure than the image end-members, thereby reducing the number of non-unique solutions. Future work will involve testing this type of calibration using the AVIRIS images, as well as further constraining the mixture model.

REFERENCES

- Adams, J.B., M.O. Smith, and P.E. Johnson, 1986, "Spectral mixture modeling: a new analysis of rock and soil types at Viking Lander 1," *J. Geophysical Research*, vol. 91, pp. 8113-8125.
- Gamon, J., C.B. Field, D.A. Roberts, S.L. Ustin, and R. Valentini, 1993, "Functional Patterns in an Annual Grassland during an AVIRIS Overflight," *Rem. Sens. Env.*, vol. 44, pp. 239-253.
- Kruse, F.A., A.B. Lekhoff, and J.B. Dietz, 1993, "Expert System-Based Mineral Mapping in Northern Death Valley, California/Nevada, Using the Airborne Visible/Infrared Imaging Spectrometer (AVIRIS)," *Rem. Sens. Env.*, vol. 44, pp. 309-335.
- Mustard, J.F., 1993, "Relationships of Soil, Grass, and Bedrock Over the Kaweah Serpentine Melange through Spectral Mixture Analysis of AVIRIS Data," *Rem. Sens. Env.*, vol. 44, pp. 293-308.
- Pieters, C.M., 1991, "Bullialdus: Strengthening the case for lunar plutons," *Geophys. Res. Lett.*, vol. 18, pp. 2129-2132.
- Roberts, D.A., M.O. Smith, and J.B. Adams, 1993, "Green Vegetation, Non photosynthetic Vegetation, and Soils in AVIRIS Data," *Rem. Sens. Env.*, vol. 44, pp. 254-269.
- Smith, M.O., S.L. Ustin, J.B. Adams, and A.R. Gillespie, 1990, "Vegetation in deserts: I. A regional measure of abundance from multispectral images," *Remote Sensing of Environment*, vol. 31, pp. 1-26.
- Tarantola and Valette, 1982, "Generalized nonlinear inverse problems solved using the least squares criterion," *Rev. Geophys. Space. Phys.*, vol. 20, pp. 219-232.
- Tompkins, S., C.M. Pieters, J.F. Mustard, and P. Pinet, 1992, "Distribution of the materials around the lunar crater Bullialdus: A spectral mixing analysis" (abstract), *Lunar Planet. Sci. XXIII*, pp. 1435-1436.
- Tompkins, S.T., J.F. Mustard, C.M. Pieters, and D.W. Forsyth, 1993, "Objective determination of image end-members in spectral mixture analysis" (abstract), *Lunar Planet. Sci. XXIV*, pp. 1431-1432.